Biochimica et Biophysica Acta 1788 (2009) 254–266

Contents lists available at ScienceDirect

Biochimica et Biophysica Acta

journal homepage: www.elsevier.com/locate/bbamem

Review

# AFM for structure and dynamics of biomembranes

Emel I. Goksu [a], Juan M. Vanegas [b], Craig D. Blanchette [c], Wan-Chen Lin [a,b], Marjorie L. Longo [a,b,*]

[a] Department of Chemical Engineering and Materials Science, University of California, Davis, CA 95616, USA
[b] Biophysics Graduate Group, College of Biological Sciences, University of California, Davis, CA 95616, USA
[c] Biophysical and Interfacial Science Group, Chemistry and Material Science, Lawrence Livermore National Laboratory, Livermore, CA 94550, USA

ARTICLE INFO

*Article history:*
Received 27 June 2008
Received in revised form 26 August 2008
Accepted 31 August 2008
Available online 11 September 2008

*Keywords:*
Atomic force microscopy
Supported lipid bilayer
Vesicle rupture
Lipid domain
General anesthetic
Membrane protein

ABSTRACT

We review structure and dynamic measurements of biomembranes by atomic force microscopy (AFM). We focus mainly on studies involving supported lipid bilayers (SLBs), particularly formation by vesicle rupture on flat and corrugated surfaces, nucleation and growth of domains in phase-separated systems, anesthetic–lipid interactions, and protein/peptide interactions in multicomponent systems. We show that carefully designed experiments along with real-time AFM imaging with superior lateral and z resolution (0.1 nm) have revealed quantitative details of the mechanisms and factors controlling vesicle rupture, domain shape and size, phase transformations, and some model biological interactions. The AFM tip can also be used as a mechanical transducer and incorporated in electrochemical measurements of membrane components; therefore, we touch on these important applications in both model and cell membranes.



**Contents**



## 1. Introduction

The atomic force microscope (AFM), a member of the family of scanning probe microscopes, was developed to image non-conducting samples which differ from its counterpart: the scanning tunneling microscope. AFM uses a microscale cantilever with a fine tip to scan the surface of the samples and the deflection of the cantilever is utilized to get information about the surface properties. The working principles and imaging modes of AFM, which are out of the scope of this review, are described in detail elsewhere [1–4]. With its incredible resolution and three-dimensional imaging capability, AFM has become an essential tool in investigating the structure and function of organic thin films, including biomembranes [4–10]. Major advantages for biomembrane samples include routine imaging in an aqueous environment, lateral resolution of several nanometers

* Corresponding author. Department of Chemical Engineering and Materials Science, University of California, Davis, CA 95616, USA. Tel.: +1 530 754 6348; fax: +1 530 752 1031.
*E-mail address:* mllongo@ucdavis.edu (M.L. Longo).

0005-2736/$ – see front matter © 2008 Elsevier B.V. All rights reserved.
doi:10.1016/j.bbamem.2008.08.021

and height resolution of 0.1 nm, and complete image formation times on the order of 1 min. In addition, unlike averaging techniques such as X-ray diffraction, local structure is obtained by AFM and only microgram quantities are required. A major limitation is that the AFM tip is capable of acting as a "molecular broom" pushing aside or damaging non-rigid or unsecured membrane and membrane components [11–14]. In order to overcome this limitation, lower forces have been employed using AFM methods such as tapping mode [15–17] and/or the biomembrane sample has been secured, e.g. by adsorption or suction onto a rigid support.

Supported lipid bilayers (SLBs) and monolayers were readily adopted for high-resolution AFM imaging [18–20]. Combining AFM data with data from other techniques, often fluorescence microscopy [18,21,22], and other model membrane systems, such as giant unilamellar vesicles (GUVs) [23,24], has revealed detail at multiple length and time-scales of complex behavior such as lipid phase separation and protein–lipid interactions. Given the potential and wide use of SLBs in biomembrane research, it is both interesting and necessary to understand the factors controlling their formation and microstructure. Therefore, we will focus in Section 2 of this review on dynamic AFM studies of vesicle rupture that have been critical to quantitative modeling of the process and developing mechanisms. Generally, flat substrates are utilized for SLB formation by vesicle rupture, but we will also cover AFM studies that used corrugated or porous substrates. Microstructure is of particular interest in SLBs containing multiple components that phase separate as models of compartmentalization or lipid rafts in cell membranes. In Section 3, we will focus on dynamic AFM studies of multicomponent vesicle rupture and phase separation necessary for understanding the factors that control the microstructures observed in these systems. For a detailed protocol of forming and AFM imaging of multicomponent supported lipid bilayers, the reader is directed to our book chapter [25].

In Section 4, we discuss "applications" of AFM in biomembranes. Thanks to the flexibility of the apparatus, AFM is not limited to model membranes and has been widely used to study real cells and their membrane components. Many groups have successfully imaged cells with AFM [26–29] in order to obtain high-resolution data that may not be attainable with other techniques such as fluorescence microscopy. We limit the discussion to the study of general anesthetics interacting with lipid bilayers using SLBs and yeast cells and peptide/protein interaction with lipid bilayers using multicomponent SLBs. Finally, AFM is not limited to imaging alone and therefore we finish the article with recent advances in electrophysiology combined with AFM, which serves as a good example of new creative approaches that take advantage of nanotechnology. The focus is on cell measurements; however these new techniques may soon see application in model membranes such as GUVs and SLBs as their development advances. The AFM has been utilized for force–distance measurements to investigate the effect of temperature [30], ion-binding and chemical structure of phospholipids [31] on the nanomechanics of lipid bilayers and the investigation of temperature-induced phase transitions in bilayers [32]. This aspect of the AFM studies was comprehensively reviewed in the work of Butt et al. [33] and in a previous review, we focused on force measurements in biomembranes using AFM [34].

## 2. SLB formation studied by AFM

### 2.1. Vesicle rupture on flat surfaces

Formation of supported lipid bilayers (SLBs) from vesicles has been one of the most encountered procedures in biomembrane studies [35,36]. This process involves the preparation of unilamellar vesicles via sonication or extrusion followed by vesicle adsorption on the surface of the support. The adsorbed vesicles, afterwards, can either fuse together to form larger vesicles, and then rupture or they can directly rupture and form SLBs on the surface. Once the vesicles are adsorbed to the surface, AFM becomes a suitable experimental technique to investigate the process in situ and in real time since the vesicles and bilayer patches can easily be distinguished from each other by the tip at a nanometer scale.

Reviakine and Brisson [37] used this approach to study the early stages of SLB formation on mica and compared their results with previous theoretical work. Vesicle solutions of egg-phosphatidylcholine (PC) or 1,2-Dioleoyl-*sn*-Glycero-3-phosphocholine (DOPC) with different lipid concentrations and various vesicle sizes were prepared by sonication ($R$~12 nm) or by extrusion ($R$~15, 25, 50 and 100 nm). After the vesicle solutions were deposited on freshly cleaved mica substrates, the surfaces were scanned with AFM in contact mode. Reviakine and Brisson observed that the SLB formation mechanism is highly dependent on vesicle size, lipid concentration and the presence of $Ca^{2+}$ ions in the medium. The critical radius of adsorption ($R_a$) and rupture radius ($R_r$), which were previously studied theoretically [38], were experimentally determined to be ~12 nm and ~75 nm, respectively, in the absence of calcium. The sonicated vesicles ($R_a<R<R_r$) fused together and ruptured after their size exceeded $R_r$ whereas the extruded vesicles with $R<75$ nm remained stable and with $R>75$ nm ruptured to form SLBs. The $Ca^{2+}$ ions were observed to enhance vesicle rupture.

Leonenko et al. [15], on the other hand, focused more on the later stages of SLB formation by using tapping-mode AFM. They could observe three consecutive stages in SLB formation regardless of the substrate modification and presence of protein in the vesicles: localized disk-like features which are footprints of the vesicles, partial continuous coverage and complete SLB formation. Leonenko et al. observed that the rupture of sonicated DOPC vesicles occurred before the disk formation as observed in the study mentioned above, and extended SLB formation is due to the fact that the surface fills in as more vesicles are adsorbed rather than the disk migration. Although the incorporation of protein into the vesicles and changing the surface charge of mica from negative to positive did not change the mechanism observed, the rate of the SLB formation changed considerably. Jass et al. [17] worked on SLB formation on hydrophilic and hydrophobic surfaces by AFM in tapping mode (Fig. 1). The liposomes were prepared by a detergent depletion technique which results in unilamellar vesicles with diameters of 200–400 nm. They could image the vesicles spreading and flattening from the outer edges toward the center until the two bilayers stacked on top of each other. Then, the top bilayer either rolled or slid over the bottom layer and the edges joined together to form bigger patches. They could observe the same mechanism on hydrophobic surfaces with more distorted attached vesicles and uneven membrane edges. The positive effect of $Ca^{2+}$ in increasing the rate of the process was observed.

Richter et al. [39] and Richter and Brisson [40,41] worked on the possible pathways of vesicle deposition on solid surfaces by using both quartz crystal microbalance with dissipation (QCM-D) monitoring and AFM in which the former method is used for global characterization of the process with high time resolution and the latter for local organization with high spatial resolution. The vesicles were prepared by tip sonication. In this study, four different pathways which were highly dependent on the electrostatic interactions could be distinguished: (i) Positively charged vesicles ruptured individually on negatively charged supports even at low coverage, (ii) At high critical coverage, vesicles with low positive, neutral or negative charge decomposed into SLBs, (iii) At low coverage, vesicles with low positive, neutral or negative charge adsorbed but were not sufficiently deformed to auto-decompose, forming a stable vesicular layer (SVL), (iv) The adsorption was inhibited for the highest negative charge vesicles.

Egawa and Furusawa [42] studied SLB formation from PC and phosphatidylethanolamine (PE) vesicles. Electrokinetic potential of both vesicles and the mica substrate were measured and it was

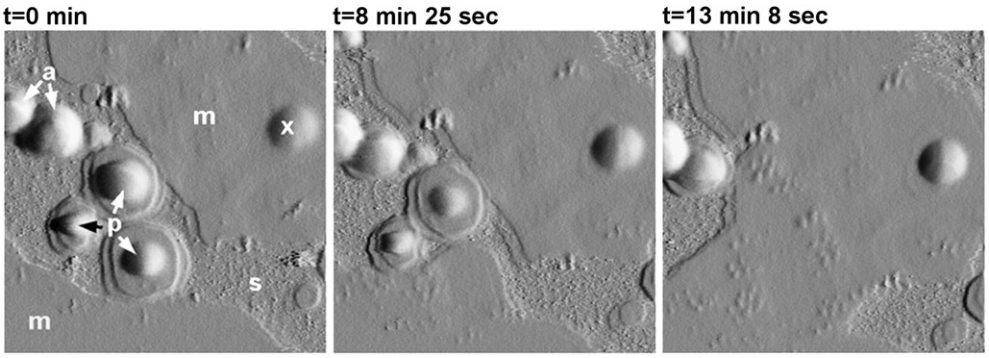


**Fig. 1.** Sequential series of AFM images presented in amplitude mode demonstrating vesicle rupture and supported lipid formation on silica. $t$=0 min, (a) attached liposomes, (p) partially flattened liposomes, (m) lipid bilayers, (s) bare silica surface, (x) a liposome that does not change throughout imaging and appears to be trapped beneath the membrane, $t$=8 min 25 s, $t$=13 min 8 s. All image sizes are 1.67×1.67 μm. Adapted from [17] with permission of the authors.

observed that even amphoteric PC vesicles have negative charges on their surfaces either due to acidic impurities and/or the hydration layers formed around the surface. In order to examine the effects of the electrostatic repulsion forces, they worked with different concentrations of $MgCl_2$ aqueous solution in which the $\zeta$-potential of the vesicles can be changed from negative values to nearly zero ($10^{-5}$ to $10^{-2}$ M). By using AFM, they could observe that bilayer coverage increases as the electrostatic repulsion forces between vesicles and mica decreases for both types of lipids. Interestingly, with PE vesicles, different from PC vesicles, there occurred double bilayer formation which could be swept away by the AFM tip scanning the surface repeatedly with high force and speed. This difference was attributed to the different hydration degrees of the membrane surfaces.

Tokumasu et al. [43] used AFM to study 1,2-Dimyristoyl-*sn*-Glycero-3-phosphocholine (DMPC) vesicle adsorption on mica at room temperature. The lipid structures in 50 mM NaCl solution were classified into three distinct groups depending on their half-width at half-maximum (HWHM) and height. By relating the obtained AFM data to the osmotic pressure relations, the lower limit of membrane elastic tensile strength for rupture was estimated to be ~4 dyn/cm. This study demonstrated the use of AFM data in determining the viscoelastic properties of membranous vesicles. Moreover, after the SLB formation, the temperature-induced melting transitions of pure DMPC SLBs were studied by raising the temperature from 18.5 °C to 32 °C during the AFM scans. The defects in the membrane decreased in size as the SLB goes from the gel phase to the liquid crystalline phase upon the temperature increase, which corresponds to an increase in the area per head group. The gel and liquid-phase thicknesses were found as ~4.2 and ~3.6 nm, respectively. The phase transition was observed to be broad over ~10 °C where gel and liquid crystalline phases coexist. Indeed, the effect of temperature in earlier stages of SLB formation was also studied using QCM-D method by Reimhult et al. [44]. Apart from the influence of surface chemistry, vesicle size and osmotic pressure on SLB formation, they have observed that vesicle rupture can take place at lower coverage of intact vesicles by the increase in temperature. Afterwards, Seantier et al. [45] demonstrated the formation of DMPC SLBs at the phase transition temperature in bulk by AFM and QCM-D, although it is often assumed that it is necessary to work over the phase transition temperatures of the lipids to form SLBs by vesicle rupture.

Other than the use of small unilamellar vesicles, Kim et al. [46] studied SLB formation from giant vesicles by AFM. When negatively charged GUVs were incubated on silica surfaces, a low surface coverage and no SLB formation were observed. The addition of $Ca^{2+}$ ions to the medium induced SLB formation. On the other hand, when the silica surface was modified such that it had a positive charge, a high surface coverage was obtained resulting in SLB formation without the addition of $Ca^{2+}$. The vesicle rupture process revealed by the AFM studies and the important factors affecting the process are summarized in Fig. 2.

### 2.2. Vesicle rupture on corrugated surfaces

Supported lipid bilayers have been successfully utilized as model cell membranes for numerous studies in the literature. However, in such a system, one of the leaflets of the SLB is not accessible for modifications. Moreover, the water layer between the membrane and the support does not provide enough space for the transmembrane proteins to be inserted leading to protein immobility. In an attempt to overcome these concerns and to study the effect of curvature on membrane properties, corrugated surfaces have been used.

AFM was utilized as a complementary method to fluorescence methods for characterization in some of these studies. For instance, Seu et al. [47] worked on the effect of surface treatment on SLB properties. DOPC/1,2-Dipalmitoyl-*sn*-Glycero-3-phosphocholine (DPPC) vesicles were prepared by the extrusion method and deposited on glass surfaces which were modified in terms of surface roughness and hydrophilicity by etching and baking. The surfaces were characterized in terms of roughness by AFM and they observed that changing the surface roughness from 0.13 to 0.26 nm did not result in a significant difference in the lateral diffusion coefficient of the lipids as compared to the hydrophilicity of the surface (the effect of hydrophilicity of the support was also previously studied by Tero et al. [48]). Apart from using AFM for support characterization, it was also used for studying SLBs on porous substrates. Steltenkamp et al. [49] used *N*,*N*,-dimethyl-*N*,*N*,-dioctadecylammonium bromide (DODAB) or 1,2-dioleoyl-3-trimethylammonium-propane chloride (DOTAP) fused vesicles prepared by extrusion to investigate the mechanical properties of the lipid bilayer suspended on pores through the analysis of force-indentation curves by solving the corresponding shape equations of continuum curvature elasticity. The substrates used were porous alumina with average pore radii of either 33±2 nm (obtained by employing oxalic acid) or 90±10 nm (obtained by anodizing aluminum in phosphoric acid). They proposed this technique as an alternative to micropipette aspiration experiments. They reported their results on the elastic properties of the lipid bilayer as a function of system geometry (tip radius and pore size) and material parameters (lateral tension and bending modulus). Gonçalves et al. [50] used a similar approach and prepared membranes spanned over nanowells leading to two aqueous chambers on each side of the membranes. They scanned the non-supported surface layers of *Corynebacterium glutamicum* and measured the elastic properties and membrane-rupture forces by using the AFM tip.

Recently, Roiter et al. [51] studied the interaction of nanoparticles with lipid membranes. In order to investigate this interaction, DMPC SLBs were formed by depositing DMPC vesicles prepared by sonication

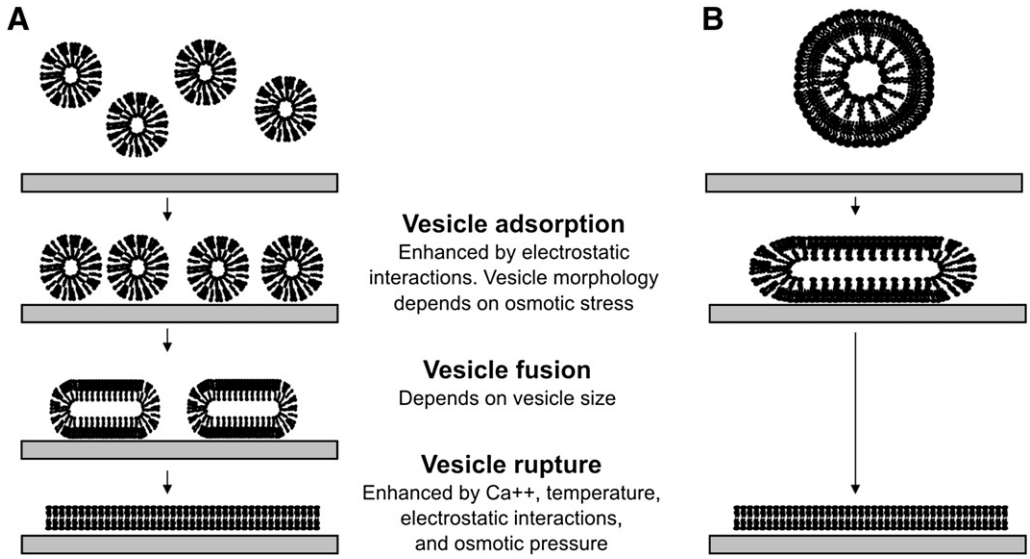


**Fig. 2.** Schematic representation of two proposed mechanisms for bilayer formation by vesicle rupture. (A) Vesicles are adsorbed on the surface, fuse together and rupture to form bilayers (B) Vesicles are adsorbed on the surface and rupture to form bilayers. The bilayer formation process is dependent on electrostatic interactions between the vesicles and support [39–42,46], vesicle size [37], osmotic stress [43], presence of $Ca^{2+}$ ions [17,37,46] and temperature [44].

onto silica nanoparticles of various sizes. By using AFM, they observed that the bilayer covers the surface of the nanoparticles having diameters larger than 22 nm or smaller than 1.2 nm. However, for particles with sizes of 1.2–22 nm, the bilayer formed pores centered at the particle center because of the curvature effect. These findings may be useful in understanding nanoparticle cytotoxicity and preparation of biomolecular templates.

Weng et al. [52,53] used QCM-D and Fluorescence Recovery After Photobleaching (FRAP) techniques to characterize the formation of SLBs from egg-PC vesicles prepared by extrusion on nanoporous xerogel and aerogel surfaces synthesized via sol-gel process. The surface structures of the substrates were characterized by SEM. They observed that the lateral diffusion coefficient of the lipids decreased as the porosity of the substrate increased. This result was attributed to the fact that the bilayer might follow the surface roughness. Goksu et al. [54] recently followed up on these results, applying AFM to characterize the surface contours of phase-separated SLBs on silica xerogels vs. mica SLBs which are smooth. They observed that both the fluid phase and gel phase lipids follow the xerogel surface contours by both contact and tapping-mode AFM. Using fluorescence techniques, they verified this by showing that the fluid phase lipid bilayer penetrates into the pores rather than being smoothly suspended on the xerogel. The bilayer following the surface roughness accounts for most of the reduction in the diffusion coefficient studied by FRAP and Fluorescence Correlation Spectroscopy (FCS).

The bilayer formation on corrugated surfaces is illustrated in Fig. 3. There are other studies in the literature on the vesicle rupture on functionalized surfaces such as tethered lipid bilayers. This aspect of the AFM studies is outside the scope of this review paper, however, the interested readers can read these references [55–59].

## 3. Multicomponent and phase-separated SLB formation studied by AFM

### 3.1. Vesicle rupture on flat substrates

The phase behavior of complex lipid mixtures has been extensively studied in the last 30 years. The phase diagrams for binary and ternary phospholipid mixtures have been determined using both theoretical [60–62] and experimental approaches, such as differential scanning calorimetry [63,64], fluorescence spectroscopy [65], NMR [66,67], X-ray diffraction [68], and electron spin resonance [69]. When lipids undergo a phase transition from a disordered to ordered state, whether it is the liquid-disordered ($L_d$)–solid ($S_o$) or the $L_d$–liquid-ordered phase ($L_o$) (when cholesterol is present) transition, the lipids will pack and extend resulting in an increase

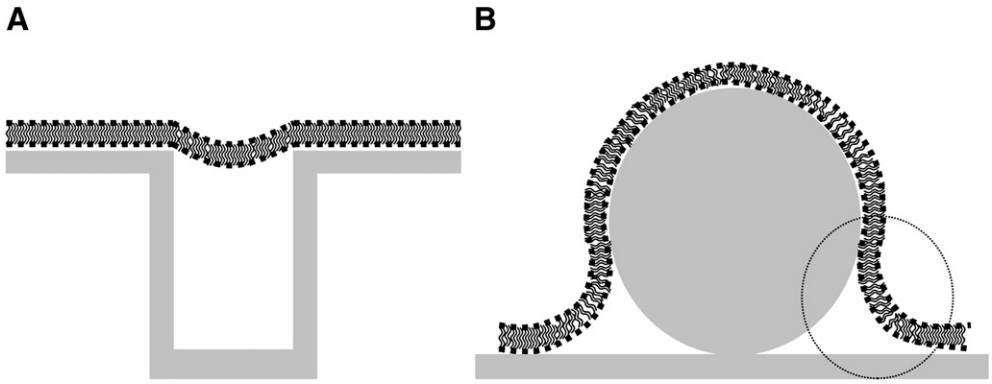


**Fig. 3.** Schematic representation of bilayers on corrugated surfaces. Continuous bilayer formation is dependent on the size of the surface features. (A) Bilayer suspended on nanowells [50], this system was also used for studying the mechanical properties of the bilayer by AFM [49]. (B) Bilayer formation on nanobeads, the encircled area is speculative since it could not be resolved by AFM [51].

in the bilayer thickness. Therefore, in phase-separated bilayers the more ordered phase will extend above the more disordered phase by approximately 0.5–2 nm. Two model membrane systems that have been extensively used to study lipid phase separation are giant unilamellar vesicles (GUVs) [23,70–72] and SLBs [73–81]. As described in the previous section, SLBs can be formed by depositing a suspension of small unilamellar vesicles (SUVs) containing the phase-separated lipid composition of interest onto an appropriate substrate where these SUVs will rupture and form a uniform two-dimensional bilayer with a ~1 nm water layer separating the bilayer from the substrate. Therefore, the two-dimensional properties of SLBs in combination with the increased thickness of the more ordered lipid phase allows for high-resolution imaging of phase-separated lipid domains by atomic force microscopy. In fact many studies have been conducted in which phase-separated domains in SLB have been imaged by AFM [71,76,79,80,82–89].

Seantier et al. [45] studied the formation of DMPC/DPPC SLBs close to the transition temperature by AFM and QCM-D. Vesicles with DMPC/DPPC ratios of 70/30 and 50/50 with transition temperatures of 29 °C and 33 °C, respectively, were prepared by tip sonication resulting in a diameter of approximately 50 nm. For these mixtures, the ambient temperature (24 °C) at which the AFM experiments were conducted falls between the pre-transition and main transition temperatures of the lipid mixture in bulk phase. AFM scans revealed that, for the 70/30 mixture, complete surface coverage was observed and the rate of SLB formation was faster compared to the 50/50 mixture for which a second injection of vesicles was needed. QCM-D experiments showed that the behaviors of both mixtures were indistinguishable at 37 °C in contrast to the experiments carried out at 24 °C. The results demonstrated that in situ kinetics of the SLB formation is highly dependent on the difference between the experimental temperature and transition temperature of the lipid mixture.

AFM has been used to characterize and study lipid bilayer symmetry in multicomponent SLB systems. In a 1,2-Dilauroyl-*sn*-Glycero-3-phosphocholine (DLPC ($T_m$=−1 °C))/1,2-Distearoyl-*sn*-Glycero-3-Phosphocholine (DSPC ($T_m$=55 °C)) system, it was found that cycling the temperature of the SUVs above and below the $T_m$ of DSPC before deposition onto a mica substrate at room temperature resulted in the formation of DSPC domains of heights extending 1.8 nm above the surrounding fluid phase [21]. It was hypothesized that temperature cycling of the SUVs promoted interleaflet mixing and that the symmetric DLPC/DSPC distribution in the SUV leaflets was maintained during and after vesicle rupture. When the DLPC/DSPC SUV temperature was held at room temperature prior to vesicle rupture, DSPC domain heights extended 1.1 nm above the surrounding fluid phase, indicating DSPC domains in one leaflet, asymmetric lipid distribution. An intermediate situation, mixed symmetry (domains with portions extending both 1.8 nm and 1.1 nm), was attained by only heating the SUVs but not cycling the temperature. The mixed symmetry lipid bilayer converted over a period of hours to either an asymmetric lipid bilayer (1.1 nm) or a symmetric bilayer (1.8 nm). Fig. 4 shows conversion from a mixed symmetry to a symmetric bilayer. Interestingly, the thickness is slightly more by about 0.4 nm on average where this new symmetric domain exists compared to the neighboring symmetric domain suggesting a difference in packing or DLPC content in the DSPC region. AFM was used to study the dynamics of the conversion. Kinetic analysis of the AFM data revealed that lipid flip-flop at the interface between symmetric and asymmetric domain regions was controlling the rate of conversion. Using AFM imaging, the same trend with respect to domain height, thermal history, and lipid flip-flop was observed when combining the observations of Choucair et al. and Giocondi et al. [90,91]. These studies show that although domains are generally "pinned" in SLBs, dynamic lipid/protein exchange and adsorption processes still readily occur as we shall see below in Sections 3.2 and 4.

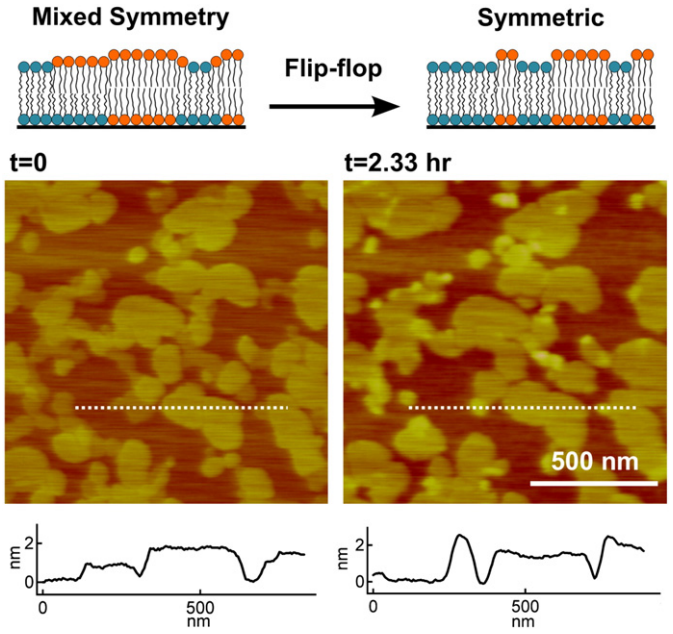


**Fig. 4.** AFM images presented in height mode of a mixed symmetry DLPC/DSPC supported lipid bilayer converting to a symmetric bilayer at $t$=0 min and $t$=2.33 h. Section analysis (dotted lines) demonstrate that two heights (~1.1 nm and ~1.8 nm) extend above the surrounding DLPC-rich region for the left image corresponding to asymmetric and symmetrically distributed DSPC. In the right image the 1.1 nm height no longer appears and instead ~2.2 nm heights appear over part of the same region, interpreted as conversion to symmetric (i.e. DSPC in registry) with a different packing in the newly created regions.

### *3.2. Domain nucleation and growth in multicomponent phase-separated SLBs*

Since capturing both domain nucleation and slight microstructure shape changes during domain growth requires high-resolution imaging techniques, AFM is optimally suited for these measurements in SLBs. Giocondi et al. [91] conducted some of the earliest measurements of real-time domain growth/rearrangement for $S_o/L_d$ phase-separated SLBs consisting of DOPC ($L_d$ phase lipid) and DPPC ($S_o$ phase lipid). In this study, the SLB was rapidly quenched from 60 to 23 °C and the time-dependent evolution of domain size and shape was imaged by AFM 19 min after the temperature quench. From this analysis, DPPC-rich domains were shown to grow by Ostwald ripening according to a power law for up to 45 min, after which the growth rate was significantly reduced.

Recently in a study by Blanchette et al. [82], steady state domain nucleation rates as a function of temperature for two different binary lipid systems, DOPC:Galactosylceramide (GalCer) and DOPC:DSPC, were determined by high-resolution AFM imaging. These two phase-separated binary mixtures differed in that DSPC domains were prepared such that each leaflet was in complete registry [73] (referred to as symmetric domains) and GalCer domains existed in only the leaflet distal to the substrate [80] (referred to as asymmetric domains). By applying classical theory of nucleation to the relatively slower DSPC and relatively faster GalCer domain nucleation rates, line tension, $\gamma$, was determined. From this analysis, $\gamma$ for symmetric DSPC domains and asymmetric GalCer domains was calculated to be 3.1±0.3 pN and 1.7±0.25 pN, respectively. Interestingly, these values were in agreement, within the same order of magnitude, with theoretical analysis [92], and in close agreement to recent experimental measurements employing shape analysis of lipid domains of GUVs held in micropipettes [23]. In addition, the relative magnitude corresponded accurately with the different hydrophobic mismatches between these symmetric and asymmetric domains, 1.8 nm and 0.9 nm respectively. More recently, by the same AFM method, Blanchette et al. [83] examined the

effect of chol on $\gamma$ in three ternary lipid mixtures consisting of 1-Palmitoyl-2-Oleoyl-*sn*-Glycero-3-phosphocholine (POPC), DLPC or DOPC, GalCer and chol. Those results implied that $\gamma$ in ordered lipid domains in ternary systems is regulated by chol concentration and the degree of regulation largely depends on the fluid phase composition which controls the partitioning. The domain nucleation work, and the recent work of Schwille's group [93] that monitored domain size as an indication of nucleation rate, roughly tested the relationship between $\gamma$ and domain height mismatch (measured by AFM) in addition to mechanical properties developed by Chizmadzhev et al. [94]. In the first case, the quadratic relationship between domain height and $\gamma$ predicted by Chizmadzhev was observed and in the second case a linear relationship was observed.

Subsequent studies focused on understanding the effect of domain symmetry on the second stage in the formation of lipid domains: the kinetics of lipid domain growth [84]. Using the same binary lipid systems described above (DOPC:GalCer and DOPC:DSPC), the fraction ($\chi_{gel}$) of GalCer or DSPC that had solidified from the fluid phase as a function of time was determined through AFM imaging during domain growth [84] (Fig. 5). Kinetics of domain growth were quantified using a reaction-diffusion model of form $\chi_{gel}=1-\exp -(kt^n)$. Interestingly, the calculated values for the kinetic exponent, $n$, show that the mechanism of domain growth depends on lipid composition and temperature, where symmetric DSPC domain growth at 1 °C and 3 °C below the liquidus temperature was reaction-limited ($n\sim2$), asymmetric GalCer domain growth at 5 °C below the liquidus temperature was diffusion-limited ($n\sim1$), and growth for the remaining conditions were controlled by both diffusion and reaction ($n$: 1.3–1.5). In agreement with the kinetic analysis, when domain growth was reaction limited (i.e. limited by lipid attachment), domains tended to grow as relatively compact round microstructures (see Fig. 5A). Fractal domain microstructures (high shape factors) grew in the diffusion-limited process. When these two processes (reaction vs. diffusion) were competing (i.e. rates of each step are similar) the observed morphologies were in between these two extreme cases (see Fig. 5B). As noticed first by Giocondi et al. [91] symmetric domain growth is slow because growth only occurs where lipids in both leaflets arrive at the same time to the growing domain.

The combined results of the studies outlined in this section have revealed insight into understanding the parameters that control phase-separated lipid domain formation in SLBs. The results from this study suggest that domain nucleation rate and growth mechanism are tightly correlated with lipid composition, domain symmetry, and temperature. The methods outlined in these studies can be readily applied to study a wider range of lipid compositions offering the potential to further understand these parameters across a greater range lipid phases.

## 4. Applications of AFM in biomembranes

### *4.1. Lipid–anesthetic interactions and interdigitation studied using SLBs and Yeasts*

Although the mechanism of action of general anesthetics is not completely understood, there have been significant advances since Meyer and Overton [95–97] first described the correlation between lipid solubility and anesthetic potency. Volatile anesthetics may exert their effects by targeting specific membrane proteins such as ligand-gated ion channels [98–100]. Cantor [101–103] has also hypothesized that anesthetics may indirectly interact with these proteins through changes in the physical properties of the lipid membrane. Many small molecules, including short-chain alcohols like ethanol, can act as anesthetics at correct doses. Alcohols are known to cause changes in the phase transitions of PCs [104–106] as well as inducing the formation of an interdigitated phase of reduced thickness (Fig. 6) [107]. In this interdigitated phase, the hydrophobic tails of the top and bottom lipids intercalate causing an increase in the area per lipid as well as the solvent exposed surface of the headgroups (see [108] for more on lipid interdigitation). The effectiveness of these alcohols at perturbing model membranes has been experimentally shown to

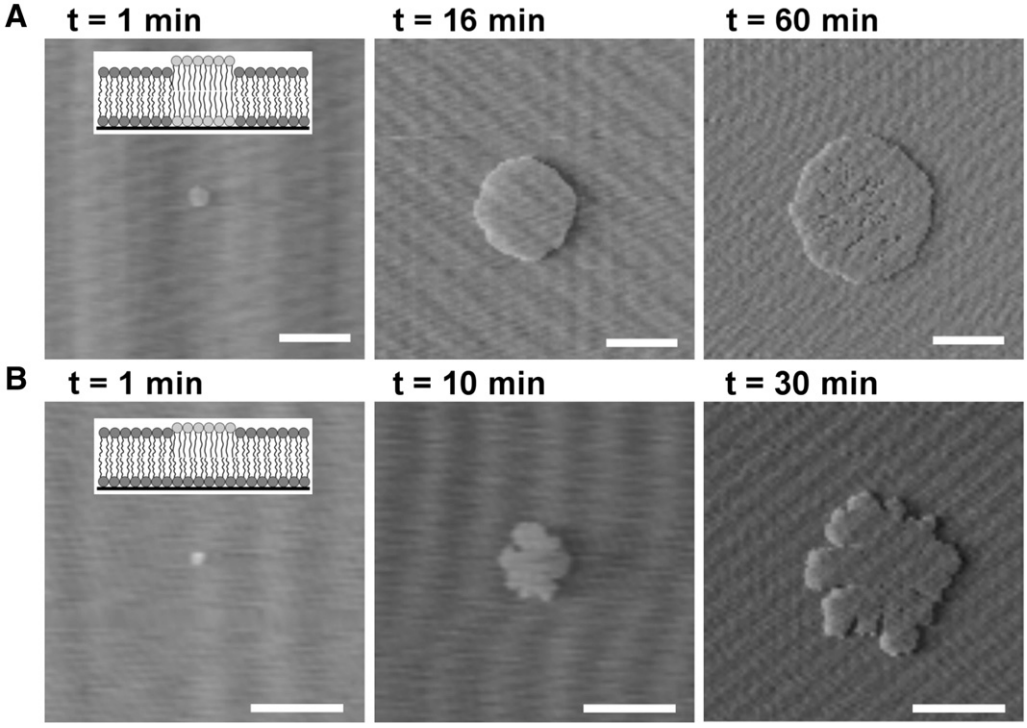


**Fig. 5.** Sequential series of AFM images presented in deflection mode demonstrating DSPC domain growth upon quenching to (A) held at 1 °C below liquidus temperature at $t=1$, 16, 60 min in a DOPC/DSPC supported lipid bilayer, note the rounded growth. (B) held at 4 °C below liquidus temperature at $t=1$, 10, 30 min in a DOPC/DSPC supported lipid bilayer, note the more leafy growth. Scale bar 5 μm.

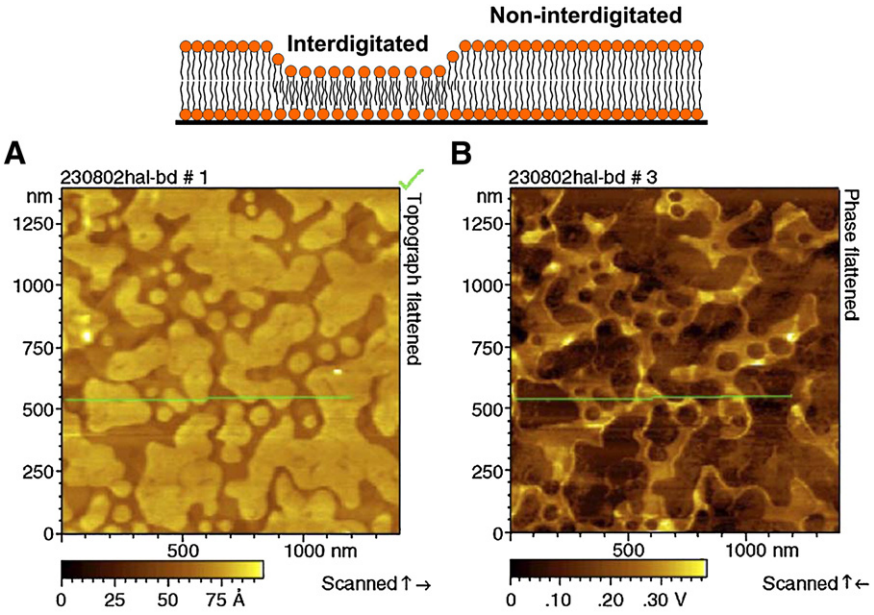


**Fig. 6.** Mac-mode AFM topography (A) and phase (B) images of a DPPC bilayer with halothane incorporated. Changes in the phase image represent changes in the viscoelasticity of the bilayer. Interdigitated domains differ in height and fluidity with respect to the gel phase. Adapted from [117] with permission of the authors.

depend on the hydrocarbon chain-length [109], which has also been confirmed by molecular dynamics simulations [110,111].

Mou et al. [112] conducted the first AFM study of alcohol-induced lipid interdigitation in 1994. In this study SLBs composed of DPPC and DSPC were exposed to ethanol and 2-propanol. In the presence of ethanol at room temperature (DPPC $T_m$=41 °C, DSPC $T_m$=55 °C), Mou et al. saw no changes in the SLB features, and only a high ethanol concentration (~200 mg/mL=19.6% v/v) and long incubation period induced the slow formation of domains. However, after heating the DPPC or DSPC bilayers above their respective $T_m$ and cooling down to room temperature, domain formation was clearly seen. These interdigitated domains remained stable even after removal of the ethanol solution, and only heating above the $T_m$ restored the normal bilayer structure. A later report by McClain and Breen [113] showed that the transition from anesthetic-induced interdigitation to gel phase can be accelerated by interaction with the AFM probe. Unilamellar DPPC SLBs were incubated (heated above $T_m$ and cooled down) with 2-propanol and imaged using cantilevers with high spring constants (an order of magnitude higher than what is normally used for these type of samples). The high imaging force supplied by the stiffer cantilever was able to reproducibly restore the bilayer to its native structure. Using this effect, McClain and Breen obtained a lipid area per headgroup of interdigitated DPPC of 90±10 Å$^2$ compared to the anesthetic-free area of 52 Å$^2$ reported elsewhere.

More recently, David Cramb's group at the University of Calgary in Canada has carried out extensive work on the interaction of the anesthetic halothane with DPPC and DOPC lipids [114–117]. The initial work by Leonenko and Cramb [114] showed that the effects of halothane at room temperature are very similar to those produced by ethanol; high concentrations of halothane induce formation of domains of similar thickness as ethanol-induced interdigitated DOPC and DPPC bilayers. However, the interaction of the lipids with the two anesthetics is different. Increasing the temperature of an ethanol-induced interdigitated DPPC SLB drives the ethanol out of the SLB and restores the SLB thickness above $T_m$. On the other hand, increasing the temperature in the halothane treated DPPC SLB extends the domain formation and increases the halothane partitioning within the SLB. The authors suggested that ethanol and halothane incorporation may have a common mechanism and is likely to be a cooperative process. A companion report by Carnini et al. [115] utilized fluorescence spectroscopy and differential scanning calorimetry of DOPC and DPPC unilamellar and multilamellar vesicles to complement the AFM results. By exploring changes in the intensity as well as wavelength shifts caused by changes in the local environment of the fluorescent lipids, Carnini et al. characterized the phase transition changes induced by halothane. Their results show that halothane increases the lipid bilayer disorder as seen by the significantly reduced DPPC melting temperature as well as the broadened transition, and they also indicate that the anesthetic partitions on the acyl chain side near the headgroup region. In a later work, Shamrakov and Cramb [116] used AFM to show that halothane induces curvature in a liquid-phase DOPC SLB. This increase in the curvature of the SLBs leads to the formation of lipid aggregates on top of the SLBs and also prevents the rupture of vesicles onto mica supports. Although the interdigitated domain formation of DPPC SLBs appears to be very similar to a gel–liquid-phase transition, the interdigitated phase has different physical properties as reported by Leonenko et al. [117]. AFM phase images of halothane treated DPPC SLBs (Fig. 6) illustrate that whereas the interdigitated domains have a reduced thickness similar to the liquid-phase DPPC, the structure and fluidity of these interdigitated domains may be different from the liquid phase. Observed adhesion forces indicate that the presence of halothane increases the fluidity of interdigitated DPPC domains, yet the values are significantly different from DPPC in the liquid phase. In addition to this, the repulsive force results suggest that halothane reduces the electrostatic shielding from water molecules and changes the surface charge density of the SLB.

A single mechanism by which all anesthetic compounds produce their effects may not be possible as some of these molecules can greatly vary in size and chemical groups. However, as seen in the case of ethanol and halothane, both molecules cause similar effects on model membranes, mainly the induction of an interdigitated phase of reduced thickness. This physical change in a cell membrane may have adverse effects on membrane-embedded proteins. As the thickness of the bilayer decreases, the hydrophobic core residues of membrane proteins may no longer be matched by the hydrophobic tails, which in turn can cause changes in the structure and activity of these proteins. So far, AFM has only been used to study the effects of anesthetics on model membranes containing one or two types of lipids. In the future, we may see similar studies with more complex mixtures that include

other lipids such as cholesterol and the inclusion of membrane proteins such as ion channels.

The effects of alcohols on membranes are not only relevant to general anesthetic mechanisms, but they are also important in the fermentation and biofuel industry. Ethanol toxicity is a major environmental stress on yeasts used in fermentation processes, and can decrease cell growth rates and viability [118]. Canetta et al. [119] used AFM to directly observe changes in surface morphology of yeast cells caused by ethanol. Two yeast strains which have different ethanol stress tolerance were analyzed: *Saccharomyces cerevisiae* and *Schizosaccharomyces pombe*. Canetta et al. measured cell volumes and roughness after exposure to ethanol at various concentrations and different exposure times. The tapping-mode AFM images show that ethanol causes the cells to shrink and makes the cell surfaces rougher. Surface roughness of both yeast strains more than doubled for the highest ethanol treatment (30% v/v, 60 min), and cell volume decreased by 35% for *S. cerevisiae* and by 50% for *S. pombe* compared to unstressed cells. The viability of these cells was 0% for this treatment. Their results confirmed previous findings which observed that *S. cerevisiae* has a higher ethanol tolerance than *S. pombe*, and indicate that stronger stresses increase alterations in the cell membrane integrity.

### 4.2. Peptide and protein-bilayer interactions in multicomponent SLBs

Another application of AFM arises due to the significance of interactions of small peptides and proteins with lipid membranes which play a role in signal transduction, toxicity, pore formation and some diseases such as Alzheimer's and Parkinson's diseases. AFM has been utilized as a convenient tool in the literature to enlighten the details of these interactions and help to understand the underlying mechanisms by either tracing the modifications in the SLB upon the addition of peptides or proteins or by measuring the interactions directly utilizing force–distance curves. The studies on peptide–lipid as well as protein–lipid interactions in multicomponent SLBs studied by AFM are summarized below and some of them are represented schematically in Fig. 7.

Kirat et al. [120] studied the effects of negatively curved lipids on the interaction of simian immunodeficiency virus (SIV) fusion peptide with model membranes. DOPC/DPPC/1,2-Dioleoyl-*sn*-Glycero-3-phosphatidic acid (DOPA, a negatively curved lipid) SLBs were incubated with SIV peptide and imaged by AFM in real time. They have observed that, after a short incubation time, the thickness of the DPPC domains decreased. However, at the end of a long incubation time, the DPPC domains converted to elevated domains which were composed of nanorod structures. These features were attributed to cylindrical reverse micelles. The presence of only negatively curved lipids was not sufficient to form reverse micelles, whereas the presence of the peptides induced the process. Andre et al. [121] also studied the interaction of hydrophobic SIV peptide with phase-separated SLBs. The peptides were attached to AFM tips and the force–distance curves were recorded upon the approach and retraction of the tip to the SLBs. In contradiction to hydrophobicity and biological functions of the peptides, a long-range repulsion upon approach and a lack of adhesion upon retraction were observed suggesting that the tip was coated with a lipid film following the first contact with SLBs. Carneiro et al. [122] worked on the interaction of vesicular stomatitis virus (VSV) with various SLB lipids at different compositions and pH values by operating the AFM in the force spectroscopy mode. They found that the binding forces are highly dependent on the phospholipid composition. The peptide–SLB interaction at pH 7.5 was specific to PS and dependent on the presence of histidine residues in the fusion peptide. Choucair et al. [90] studied the interaction of β-amyloid (Aβ) peptides with phase-separated DOPC/DPPC SLBs by AFM and total internal reflection fluorescence microscopy (TIRF). By AFM, it was observed that the addition of the peptides resulted in the preferential formation of aggregates on symmetric gel phase DPPC domains. However, when the peptides were added to the vesicles prior to the formation of SLB, Aβ was randomly distributed in both fluid and gel phases. These results may be related with the possible role of lipid rafts in the enhancement of Aβ aggregation and in modulating the Aβ activity in vivo. García-Sáez et al. [123] worked on the interaction of Bax (a critical regulator of cell death that increases the outer membrane permeability in mitochondria) with phase-separated DOPC/SM/Cholesterol SLBs by confocal microscopy and AFM. It was observed that the force needed to form a hole in the SLB decreased in the presence of Bax-α5. Moreover, the peptide changed the line tension between the phases and the liquid-ordered domains lost their circular shape and expanded in size. This change in line tension

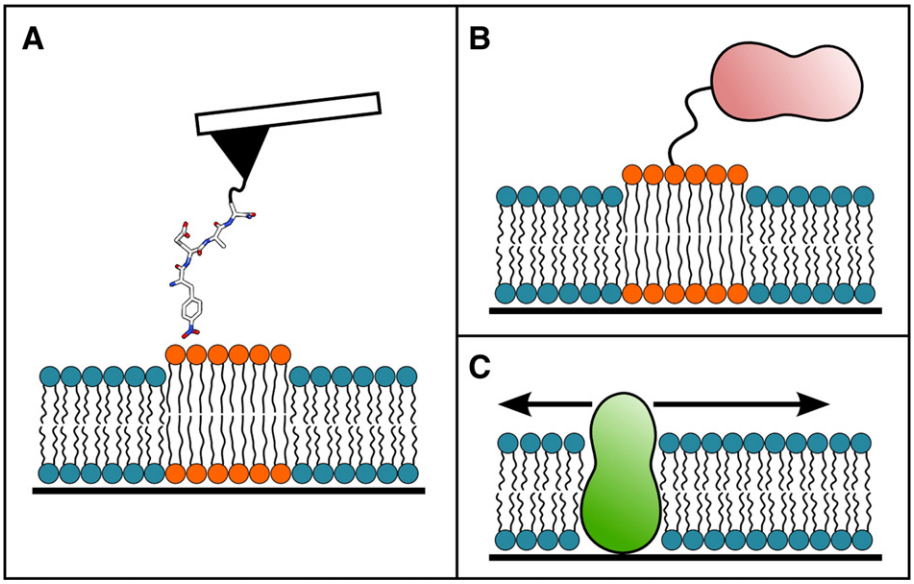


**Fig. 7.** Schematic representation of peptide/protein–lipid interactions studied by AFM. (A) Peptide was attached to the tip to measure lipid–peptide interactions [121]. (B) GPI-anchored BIAP proteins were observed to insert into the ordered domains [127,128]. (C) Lateral diffusion coefficients of proteins were measured by AFM [130,131].

was thought to be a general strategy of pore forming peptides since it affects the pore formation and stabilizes the open state.

As for the protein–lipid interactions, You et al. [124,125] investigated the interactions between the Saposin C (Sap C, a small glycoprotein playing an essential role in the enzymatic activity of glucosylceramidase) and DSPC/1-Palmitoyl,2-oleoyl-*sn*-Glycero-3-phosphoserine (POPS) SLBs. It was observed that the SLB underwent restructuring upon the addition of Sap C such that there occurred patch-like new features emerging at the edge of SLB and extending with time. Moreover, image contrast changes indicated formation of a new phase of protein–lipid structure. Incorporation of raft-enriched lipids, i.e. cholesterol and sphingomyelin, into the SLB affected the modulation and control of Sap C-bilayer interactions and nanometer-sized domains were formed. Murray et al. [126] studied the binding of synapsin to phase-separated SLBs. SLBs with 1,2-Dipalmitoyl-*sn*-Glycero-3-phosphoethanolamine (DPPE) as the lower leaflet and DLPC/1,2-Dipalmitoyl-*sn*-Glycero-3-phosphoserine (DPPS) or DPPC/DPPS as the outer leaflet were prepared. By AFM, they showed that synapsin interacted with negatively charged DPPS-rich domains by electrostatic binding and PC phase by nonspecific binding. Moreover, it was observed that the PS rich domains contained within a DPPC SLB, which could not be differentiated in the topography images, were clearly observable when synapsin-coated tips were used instead.

Giocondi et al. [127] studied the effect of fluid/gel lipid composition on the interaction of glycosylphosphatidyl-inositol (GPI)-anchored proteins with membrane domains. GPI-anchored intestinal alkaline phosphatase (BIAP) spontaneously inserted into gel phase domains in DOPC/DPPC, DOPC/sphingomyelin (SM), POPC/SM lipid SLBs. However, changes in the lipid composition of the SLBs altered the topography drastically in the protein containing SLBs. BIAP insertion into the domains was associated with the transfer of lipids from the fluid to gel (DOPC/DPPC) or gel to fluid (POPC/SM) phases. In DOPC/SM SLBs, the transfer was dependent on the homogeneity of the domains. Their results strongly suggest that the insertion of BIAP depends on the membrane structure in terms of hydrophobic length and lipid order parameter. In another study by the same group [128], it was shown that BIAP was preferentially localized in the highly ordered SM/Chol enriched domains in POPC/SM/Chol bilayers. In order to determine if this behavior is related with the lipid ordering, the temperature was increased above 30 °C modifying the lipid ordering and it was observed that BIAP redistributed and was present in both fluid POPC and SM/Chol domains. The authors pointed out the fact that not detecting significant amounts of BIAP in the fluid phase at low temperatures did not mean there was no BIAP in fluid phase basing on a previous study by Chianta et al. [129]; there can be few molecules diffusing with a rate exceeding the scanning rate of AFM (therefore, two-focus FCS was coupled to AFM results to observe the fast dynamics of the proteins). On the contrary, Müller et al. [130] have previously used AFM as a technique to visualize the dynamics of the single-sodium driven rotors from a bacterial ATP synthase embedded into a lipid membrane in subnanometer resolution. They scanned considerably small areas of lipid bilayer (smaller than 0.1 $\mu m^2$) with 90 s time intervals. They could distinguish both free and obstacle diffusion of the proteins and observed that the diffusion constants of these two modes were considerably different; $2.04\times10^{-5}$ $\mu m^2/s$ and $0.32\times10^{-5}$ $\mu m^2/s$, respectively. Hughes et al. [131] used a similar approach to work on the dynamics of mobile influenza A M2 molecules in DPPC bilayers supported by mica. The lateral diffusion coefficient of the M2 was found to be $4.4\pm1.0\times10^{-14}$ $cm^2/s$ by using the mean-square displacement data.

AFM has also been used as a convenient tool in high-resolution imaging of proteins and revealed significant information about protein structures [132–134]. Hussain et al. [135] used this approach to image the fibrinogen protein and Arg-Gly-Asp (RGD) peptide ligands binding to platelet integrin αIIbβ3 receptors reconstituted into planar bilayers. Since the peptide ligands were too small, they were labeled with gold particles. The fibrinogen–integrin binding could be easily observed with fibrinogen having a characteristic trinodular structure and occasionally bridging the receptors. The interactions with peptides, on the other hand, were not observable in the height images, but the phase images which took the advantage of the mechanical properties detected the nanogold labels and showed the binding of peptides to the receptors. Milhiet et al. [136] described a new method of incorporating a high density of transmembrane proteins into bilayers which were destabilized by two different detergents at 20 °C and 4 °C. The AFM height measurements revealed that proteins were unidirectionally incorporated in the bilayer through their more hydrophobic domains. The high density of proteins led to the high-resolution AFM images of the protein subunits. This study demonstrated an alternative protocol for two-dimensional crystallization of proteins for AFM analysis.

### 4.3. Membrane electrophysiology combined with AFM

Supported lipid bilayers provide an excellent system for the study of membranes using AFM. Because the composition of the membranes can be controlled, a 'bottom-up' approach can be used to progressively study systems of higher complexity and which resemble real biological membranes. Studies of these model membranes provide understanding of fundamental aspects of very complex systems such as real cells. New creative approaches accompanied by advances in nanotechnology allow the use of techniques such as AFM to study live cells and their components in real time. Thanks to its versatility, AFM can be combined with other biophysical methods including voltage or patch-clamping. Voltage-clamping allows the electrochemical characterization of membranes and their embedded protein components by recording transmembrane currents.

Although voltage-clamping is highly sensitive to electrical changes across the membrane, it does not provide direct structural information on the surface of the clamped membrane. In an effort to overcome this limitation, various groups have successfully combined membrane patch-clamping [137,138] as well as voltage-clamping of live cells [139–141] with AFM. In the earlier work, Hörber et al. [138] excised plasma membrane patches from *Xenopus laevis* oocytes and produced different preparations that permit the imaging of both the inside and outside of the membrane. Their experimental setup allowed them to acquire AFM images while the membrane was clamped to the pipette. Images from different preparations show an underlying fiber structure (cytoskeleton) that extends from the center of the patches to the edges of the pipette. Hörber et al. also used the AFM tip to measure the elasticity of the membrane and obtained values comparable to those found in the literature. Extending this combined approach, Danker et al. [137] investigated nuclear membrane patches from the same type of oocytes in order to characterize nuclear pore complexes (NPCs). In this study patches of the isolated nuclear envelope were excised with the patch pipette and their electrical properties recorded with an electrode. Rather than imaging the patches on the pipette, the patches were 'blown out' onto a mica or glass substrate and then imaged with AFM. To their surprise, Danker et al. observed three kinds of membrane types, that had different surface morphologies or conducting properties, some of which did not contain NPCs and were designated as endoplasmic reticulum (ER). This result challenged the observations made by other groups in which similarly isolated nuclear membrane patches were regarded as ER free [137].

Using a more dynamic setup, Mosbacher et al. [139] investigated electromechanical coupling of voltage-clamped HEK293 cells transfected with mutant non-inactivating *Shaker* $K^+$ channels. In their setup, cells were clamped to the pipette while an AFM cantilever rested on top and measured the movement of the membrane (Fig. 8A). Both transfected and untransfected cells were held at a specific potential and an AC carrier signal drove the potential at a certain frequency. Mosbacher et al. observed a displacement of the cell

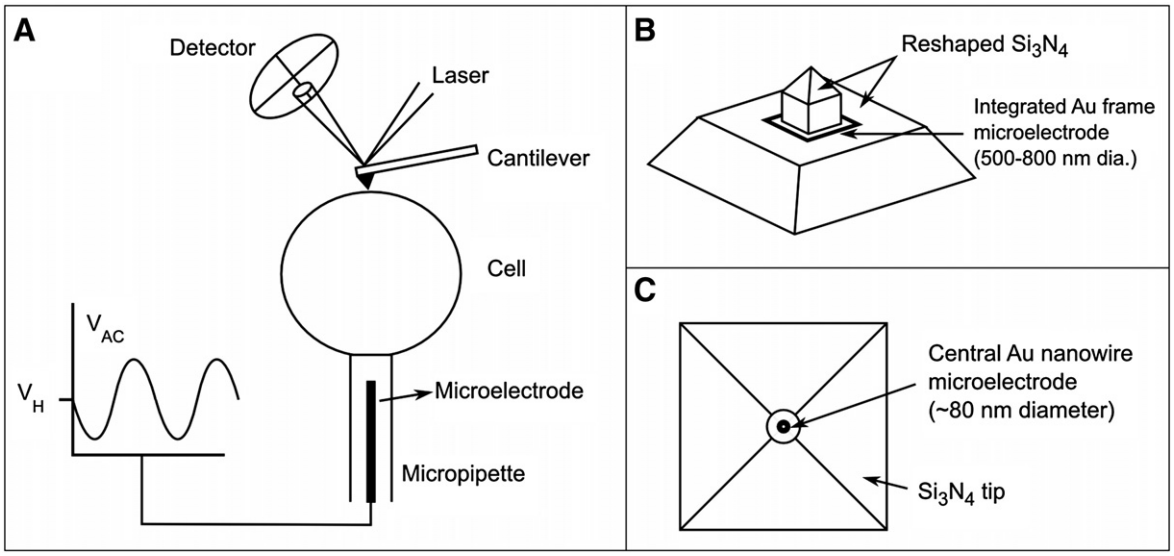


**Fig. 8.** (A) Setup for voltage-clamping of live cells used by Mosbacher et al. [139]. (B) and (C) illustrate two examples of combined SECM-AFM tips. (B) Integrated Au frame microelectrode design by Kranz et al. [149] and (C) central Au nanowire design by Burt et al. [148].

membrane which is linearly dependent on the amplitude of the AC carrier signal and possesses the same frequency of oscillation. In an unexpected result they measured displacements in both the control cells (untransfected) as well as the transfected cells. While membrane motion of the transfected cells was affected by the holding potential, untransfected cells were unaffected by it. This result shows that both the channels and the membrane respond to electromechanical changes. A mathematical model was proposed by Zhang et al. [141] in a letter to Nature which explains these observations. The model uses the Lippmann equation and is derived from thermodynamic principles, so its predictions should be applicable to all membranes [141]. Using a similar setup as Mosbacher et al., Zhang et al. confirmed that membrane tension can be modulated by transmembrane voltages, and the extent and direction of movement depends on cell stiffness as well as magnitude of the potentials.

Another technique available to study the electrochemistry of surfaces is scanning electrochemical microscopy (SECM) [142–145]. In this scanning probe technique an ultra-microelectrode, usually of micrometer dimensions, is used as the imaging tip. Although SECM provides valuable information, the acquired data is convoluted by the surface topography and reactivity, and the spatial resolution of the technique is far lower than AFM or STM due to the size of the microelectrode [146]. These limitations can be overcome by using a combined SECM-AFM probe that can provide simultaneous topography and electrical recordings. Several methods have been successfully used for the production of these probes [147–151]. However, detailed description of the construction and characteristics of these is beyond the scope of this article. It is worth noting some of the key aspects of these probes. The design by Kranz et al. [149] achieves high topographical resolution while sacrificing electrode size, yet they achieved a microelectrode diameter of only 800 nm (Fig. 8B). A nanowire probe constructed by Burt et al. [148] has a larger tip size (~400 nm in diameter) but contains a central Au nanowire ~80 nm in diameter (Fig. 8C). Simultaneous electrochemical-topographical images of synthetic [152,153] and biological [154] membranes have been obtained with some of these SECM-AFM probes. Quist et al. [154] have also devised a technique to nanofabricate silicon supports with nanopores down to 50 nm in diameter, which allow electrical recordings while providing enough support for model membranes.

Patch-clamping has proved to be an essential tool in the study of electrochemical properties of cellular membranes and their protein components. Rising new technologies, such as combined SECM-AFM can take patch-clamping to a new level. Nanofabricated SECM-AFM probes may one day be capable of recording electrical signals across individual ion channels while providing real-time structural information. This may be possible not only on supported membranes, but on live cells as well. Additionally, SECM-AFM probes may be used to monitor structural changes of membrane components during an electrochemical change such as an action potential.

## 5. Conclusions

We have limited this review on AFM to several important processes in model and cell membranes, some at the nanometer scale, including bilayer formation by vesicle rupture, domain nucleation and growth, anesthetic and protein/peptide-bilayer interactions in multicomponent bilayers, and membrane electrophysiology. The selected topics are only a fraction of the literature available on biomembranes examined by AFM, yet these topics had not been extensively reviewed elsewhere to the best of our knowledge. AFM has been successfully combined with many complementary techniques such as fluorescence microscopy and QCM-D to get high-resolution data that may not be possible to obtain using these techniques alone. An example of this complementarity is the tracking of protein movement in a membrane, where in order to access the fast diffusion dynamics, AFM was needed to be coupled to FCS. AFM is not only used to image membrane processes, but it is also used as a unique technique to probe the mechanical properties of bilayers as an alternative to micropipette aspiration. Although there have been several studies about domain nucleation and growth in multicomponent bilayers studied by AFM, with its high-resolution, future studies will likely continue to use AFM to enlighten the basic interactions between lipids. Finally, the last section on membrane electrophysiology may serve a two-fold purpose. First, to show how electrophysiology may benefit greatly from the recent advances in nanotechnology as new techniques will reduce the scale at which readings are taken and provide more selective ways of probing electrochemical properties. Secondly, to illustrate the versatility of the AFM technique and the creative approaches that investigators have taken to improve existing instrumentation.

## Acknowledgments

We acknowledge funding by the USDA (2007-02140), NSF NIRT Program (CHE 0210807 and CBET 0506602) and the NSF MRSEC

Program CPIMA (NSF DMR 0213618). This work was performed under the auspices of the U.S. Department of Energy by Lawrence Livermore National Laboratory in part under Contract W-7405-Eng-48 and in part under Contract DE-AC52-07NA27344.

## References

[1] G. Binnig, C.F. Quate, C. Gerber, Atomic force microscope, Phys. Rev. Lett. 56 (1986) 930–933.
[2] P.K. Hansma, V.B. Elings, O. Marti, C.E. Bracker, Scanning tunneling microscopy and atomic force microscopy: application to biology and technology, Science 242 (1988) 209–216.
[3] Z. Shao, J. Mou, D.M. Czajkowsky, J. Yang, J.Y. Yuan, Biological atomic force microscopy: what is achieved and what is needed, Adv. Phys. 45 (1996) 1–86.
[4] A. Alessandrini, P. Facci, AFM: a versatile tool in biophysics, Meas. Sci. Technol. 16 (2005) R65–R92.
[5] Y.F. Dufrene, G.U. Lee, Advances in the characterization of supported lipid films with the atomic force microscope, Biochim. Biophys. Acta 1509 (2000) 14–41.
[6] J.L. Alonso, W.H. Goldmann, Feeling the forces: atomic force microscopy in cell biology, Life Sci. 72 (2003) 2553–2560.
[7] L.J. Johnston, Nanoscale imaging of domains in supported lipid membranes, Langmuir 23 (2007) 5886–5895.
[8] J. Yang, AFM as a high-resolution imaging tool and a molecular bond force probe, Cell Biochem. Biophys. 41 (2004) 435–449.
[9] Y.F. Dufrêne, Using nanotechniques to explore microbial surfaces, Nat. Rev. Microbiol. 2 (2004) 451–460.
[10] N. Gadegaard, Atomic force microscopy in biology: technology and techniques, Biotech. Histochem. 81 (2006) 87–97.
[11] K. Dimitrievski, M. Zäch, V.P. Zhdanov, B. Kasemo, Imaging and manipulation of adsorbed lipid vesicles by an AFM tip: experiment and Monte Carlo simulations, Colloids Surf. B. Biointerfaces 47 (2006) 115–125.
[12] X.C. Zhao, N.O. Petersen, Z.F. Ding, Comparison study of live cells by atomic force microscopy, confocal microscopy, and scanning electrochemical microscopy, Can. J. Chem. 85 (2007) 175–183.
[13] S.L. Brandow, D.C. Turner, B.R. Ratna, B.P. Gaber, Modification of supported lipid membranes by atomic force microscopy, Biophys. J. 64 (1993) 898–902.
[14] M. Beckmann, P. Nollert, H.A. Kolb, Manipulation and molecular resolution of a phosphatidylcholine-supported planar bilayer by atomic force microscopy, J. Membr. Biol. 161 (1998) 227–233.
[15] Z.V. Leonenko, A. Carnini, D.T. Cramb, Supported planar bilayer formation by vesicle fusion: the interaction of phospholipid vesicles with surfaces and the effect of gramicidin on bilayer properties using atomic force microscopy, Biochim. Biophys. Acta 1509 (2000) 131–147.
[16] E. Giannakis, J. Pacifico, D.P. Smith, L.W. Hung, C.L. Masters, R. Cappai, J.D. Wade, K.J. Barnham, Dimeric structures of α-synuclein bind preferentially to lipid membranes, Biochim. Biophys. Acta 1178 (2008) 1112–1119.
[17] J. Jass, T. Tjärnhage, G. Puu, From liposomes to supported, planar bilayer structures on hydrophilic and hydrophobic surfaces: an atomic force microscopy study, Biophys. J. 79 (2000) 3153–3163.
[18] S. Singh, D.J. Keller, Atomic force microscopy of supported planar membrane bilayers, Biophys. J. 60 (1991) 1401–1410.
[19] Y. Fang, J. Yang, Role of the bilayer–bilayer interaction on the ripple structure of supported bilayers in solution, J. Phys. Chem. 100 (1996) 15614–15619.
[20] L.K. Tamm, C. Böhm, J. Yang, Z. Shao, J. Hwang, M. Edidin, E. Betzig, Nanostructure of supported phospholipid monolayers and bilayers by scanning probe microscopy, Thin Solid Films 284–285 (1996) 813–816.
[21] W.-C. Lin, C.D. Blanchette, T.V. Ratto, M.L. Longo, Lipid asymmetry in DLPC/DSPC-supported lipid bilayers: a combined AFM and fluorescence microscopy study, Biophys. J. 90 (2006) 228–237.
[22] J.E. Shaw, R.F. Epand, R.M. Epand, Z. Li, R. Bittman, C.M. Yip, Correlated fluorescence-atomic force microscopy of membrane domains: structure of fluorescence probes determines lipid localization, Biophys. J. 90 (2006) 2170–2178.
[23] A. Tian, C. Johnson, W. Wang, T. Baumgart, Line tension at fluid membrane domain boundaries measured by micropipette aspiration, Phys. Rev. Lett. 98 (2007) 208102.
[24] W.-C. Lin, C.D. Blanchette, M.L. Longo, Fluid-phase chain unsaturation controlling domain microstructure and phase in ternary lipid bilayers containing GalCer and cholesterol, Biophys. J. 92 (2007) 2831–2841.
[25] W.-C. Lin, C.D. Blanchette, T.V. Ratto, M.L. Longo, Lipid domains in supported lipid bilayer for atomic force microscopy, in: A. Dopico (Ed.), Protocols in Biophysics to Study Membrane Lipids, Humana Press, 2007.
[26] A. Sharma, K.I. Anderson, D.J. Müller, Actin microridges characterized by laser scanning confocal and atomic force microscopy, FEBS Lett. 579 (2005) 2001–2008.
[27] M. Murakoshi, T. Gomi, K. Iida, S. Kumano, K. Tsumoto, I. Kumagai, K. Ikeda, T. Kobayashi, H. Wada, Imaging by atomic force microscopy of the plasma membrane of prestin-transfected Chinese hamster ovary cells, J. Assoc. Res. Otolaryngol. 7 (2006) 267–278.
[28] D.J. Frankel, J.R. Pfeiffer, Z. Surviladze, A.E. Johnson, J.M. Oliver, B.S. Wilson, A.R. Burns, Revealing the topography of cellular membrane domains by combined atomic force microscopy/fluorescence imaging, Biophys. J. 90 (2006) 2404–2413.
[29] C.M. Franz, D.J. Müller, Analyzing focal adhesion structure by atomic force microscopy, J. Cell Sci. 118 (2005) 5315–5323.
[30] S. Garcia-Manyes, G. Oncins, F. Sanz, Effect of temperature on the nanomechanics of lipid bilayers studied by force spectroscopy, Biophys. J. 89 (2005) 4261–4274.
[31] S. Garcia-Manyes, G. Oncins, F. Sanz, Effect of ion-binding and chemical phospholipid structure on the nanomechanics of lipid bilayers studied by force spectroscopy, Biophys. J. 89 (2005) 1812–1826.
[32] Z.V. Leonenko, E. Finot, H. Ma, T.E.S. Dahms, D.T. Cramb, Investigation of temperature-induced phase transitions in DOPC and DPPC phospholipid bilayers using temperature-controlled scanning force microscopy, Biophys. J. 86 (2004) 3783–3793.
[33] H.J. Butt, B. Cappella, M. Kappl, Force measurements with the atomic force microscope: technique, interpretation and applications, Surf. Sci. Rep. 59 (2005) 1–152.
[34] C.D. Blanchette, T.V. Ratto, M.L. Longo, Model cell membrane surfaces for measuring receptor–ligand interactions, in: M.R. King (Ed.), Cellular Engineering: Micromechanics at the Biomolecular Interface, Elsevier Science, 2006.
[35] T.H. Watts, A.A. Brian, J.W. Kappler, P. Marrack, H.M. McConnell, Antigen presentation by supported planar membranes containing affinity-purified I-Ad, Proc. Natl. Acad. Sci. U. S. A. 81 (1984) 7564–7568.
[36] H.M. McConnell, T.H. Watts, R.M. Weis, A.A. Brian, Supported planar membranes in studies of cell–cell recognition in the immune-system, Biochim. Biophys. Acta 864 (1986) 95–106.
[37] I. Reviakine, A. Brisson, Formation of supported phospholipid bilayers from unilamellar vesicles investigated by atomic force microscopy, Langmuir 16 (2000) 1806–1815.
[38] R. Lipowsky, U. Seifert, Adhesion of membranes: a theoretical perspective, Langmuir 7 (1991) 1867–1873.
[39] R. Richter, A. Mukhopadhyay, A. Brisson, Pathways of lipid vesicle deposition on solid surfaces: a combined QCM-D and AFM study, Biophys. J. 85 (2003) 3035–3047.
[40] R.P. Richter, A. Brisson, QCM-D on mica for parallel QCM-D-AFM studies, Langmuir 20 (2004) 4609–4613.
[41] R.P. Richter, A.R. Brisson, Following the formation of supported lipid bilayers on mica: a study combining AFM, QCM-D, and ellipsometry, Biophys. J. 88 (2005) 3422–3433.
[42] H. Egawa, K. Furusawa, Liposome adhesion on mica surface studied by atomic force microscopy, Langmuir 15 (1999) 1660–1666.
[43] F. Tokumasu, A.J. Jin, G.W. Feigenson, J.A. Dvorak, Atomic force microscopy of nanometric liposome adsorption and nanoscopic membrane domain formation, Ultramicroscopy 97 (2003) 217–227.
[44] E. Reimhult, F. Hook, B. Kasemo, Intact vesicle adsorption and supported biomembrane formation from vesicles in solution: influence of surface chemistry, vesicle size, temperature, and osmotic pressure, Langmuir 19 (2003) 1681–1691.
[45] B. Seantier, C. Breffa, O. Félix, G. Decher, In situ investigations of the formation of mixed supported lipid bilayers close to the phase transition temperature, Nano Lett. 4 (2004) 5–10.
[46] Y. Kim, M. Rahman, Z. Zhang, N. Misawa, R. Tero, T. Urisu, Supported lipid bilayer formation by giant vesicle fusion induced by vesicle-surface electrostatic attractive interaction, Chem. Phys. Lett. 420 (2006) 569–573.
[47] K.J. Seu, A.P. Pandey, F. Haque, E.A. Proctor, A.E. Ribbe, J.S. Hovis, Effect of surface treatment on diffusion and domain formation in supported lipid bilayers, Biophys. J. 92 (2007) 2445–2450.
[48] R. Tero, H. Watanabe, T. Urisu, Supported phospholipid bilayer formation on hydrophilicity-controlled silicon dioxide surfaces, PCCP 8 (2006) 3885–3894.
[49] S. Steltenkamp, M.M. Müller, M. Deserno, C. Hennesthal, C. Steinem, A. Janshoff, Mechanical properties of pore-spanning lipid bilayers probed by atomic force microscopy, Biophys. J. 91 (2006) 217–226.
[50] R.P. Gonçalves, G. Agnus, P. Sens, C. Houssin, B. Bartenlian, S. Scheuring, Two-chamber AFM: probing membrane proteins separating two aqueous compartments, Nat. Methods 3 (2006) 1007–1012.
[51] Y. Roiter, M. Ornatska, A.R. Rammohan, J. Balakrishnan, D.R. Heine, S. Minko, Interaction of nanoparticles with lipid membrane, Nano Lett. 8 (2008) 941–944.
[52] K.C. Weng, J.J.R. Stalgren, D.J. Duval, S.H. Risbud, C.W. Frank, Fluid biomembranes supported on nanoporous aerogel/xerogel substrates, Langmuir 20 (2004) 7232–7239.
[53] K.C. Weng, J.J.R. Stalgren, S.H. Risbud, C.W. Frank, Planar bilayer lipid membranes supported on mesoporous aerogels, xerogels, and Vycor® glass: an epifluorescence microscopy study, J. Non-Cryst. Solids 350 (2004) 46–53.
[54] E.I. Goksu, B.A. Nellis, W.C. Lin, S.H. Risbud, M.L. Longo, Domain formation and lateral lipid diffusion in nanoporous substrate supported lipid bilayers, Biophys. J. 94 (2008) 1184.
[55] M. Seitz, E. Ter-Ovanesyan, M. Hausch, C.K. Park, J.A. Zasadzinski, R. Zentel, J.N. Israelachvili, Formation of tethered supported bilayers by vesicle fusion onto lipopolymer monolayers promoted by osmotic stress, Langmuir 16 (2000) 6067-6070.
[56] A.T.A. Jenkins, R.J. Bushby, S.D. Evans, W. Knoll, A. Offenhäusser, S.D. Ogier, Lipid vesicle fusion on μCP patterned self-assembled monolayers: effect of pattern geometry on bilayer formation, Langmuir 18 (2002) 3176–3180.
[57] A. Berquand, P. Mazeran, J. Pantigny, V. Proux-Delrouyre, J. Laval, C. Bourdillon, Two-step formation of streptavidin-supported lipid bilayers by PEG-triggered vesicle fusion. Fluorescence and atomic force microscopy characterization, Langmuir 19 (2003) 1700–1707.
[58] B.R. Dorvel, H.M. Keizer, D. Fine, J. Vuorinen, A. Dodabalapur, R.S. Duran, Formation of tethered bilayer lipid membranes on gold surfaces: QCM-Z and AFM study, Langmuir 23 (2007) 7344–7355.

[59] S.B. Lei, R. Tero, N. Misawa, S. Yamamura, L.J. Wan, T. Urisu, AFM characterization of gramicidin-A in tethered lipid membrane on silicon surface, Chem. Phys. Lett. 429 (2006) 244–249.
[60] I.P. Sugar, E. Michanova-Alexova, P.L.G. Chong, Geometrical properties of gel and fluid clusters in DMPC/DSPC bilayers: Monte Carlo simulation approach using a two-state model, Biophys. J. 81 (2001) 2425–2441.
[61] K. Jorgensen, M.M. Sperotto, O.G. Mouritsen, J.H. Ipsen, M.J. Zuckermann, Phase-equilibria and local-structure in binary lipid bilayers, Biochim. Biophys. Acta 1152 (1993) 135–145.
[62] J.H. Ipsen, O.G. Mouritsen, Modeling the phase-equilibria in 2-component membranes of phospholipids with different acyl-chain lengths, Biochim. Biophys. Acta 944 (1988) 121–134.
[63] S. Mabrey, J.M. Sturtevant, Investigation of phase-transitions of lipids and lipid mixtures by high sensitivity differential scanning calorimetry, Proc. Natl. Acad. Sci. U. S. A. 73 (1976) 3862–3866.
[64] P.W.M. Vandijck, A.J. Kaper, H.A.J. Oonk, J. Degier, Miscibility properties of binary phosphatidylcholine mixtures — calorimetric study, Biochim. Biophys. Acta 470 (1977) 58–69.
[65] B.R. Lentz, Y. Barenholz, T.E. Thompson, Fluorescence depolarization studies of phase-transitions and fluidity in phospholipid bilayers .2. 2-component phosphatidylcholine liposomes, Biochemistry 15 (1976) 4529–4537.
[66] R.J. Wittebort, A. Blume, T.H. Huang, S.K. Dasgupta, R.G. Griffin, C-13 nuclear magnetic-resonance investigations of phase-transitions and phase-equilibria in pure and mixed phospholipid-bilayers, Biochemistry 21 (1982) 3487–3502.
[67] K. Arnold, A. Losche, K. Gawrisch, P-31-NMR investigations of phase-separation in phosphatidylcholine-phosphatidylethanolamine mixtures, Biochim. Biophys. Acta 645 (1981) 143–148.
[68] M. Caffrey, F.S. Hing, A temperature-gradient method for lipid phase-diagram construction using time-resolved X-ray-diffraction, Biophys. J. 51 (1987) 37–46.
[69] E.J. Shimshic, H.M. Mcconnel, Lateral phase separation in phospholipid membranes, Biochemistry 12 (1973) 2351–2360.
[70] S.L. Veatch, S.L. Keller, Organization in lipid membranes containing cholesterol, Phys. Rev. Lett. 89 (2002).
[71] G.W. Feigenson, J.T. Buboltz, Ternary phase diagram of dipalmitoyl-PC/dilauroyl-PC/cholesterol: nanoscopic domain formation driven by cholesterol, Biophys. J. 80 (2001) 2775–2788.
[72] L.A. Bagatolli, E. Gratton, A correlation between lipid domain shape and binary phospholipid mixture composition in free standing bilayers: a two-photon fluorescence microscopy study, Biophys. J. 79 (2000) 434–447.
[73] T.V. Ratto, M.L. Longo, Obstructed diffusion in phase-separated supported lipid bilayers: a combined atomic force microscopy and fluorescence recovery after photobleaching approach, Biophys. J. 83 (2002) 3380–3392.
[74] B.L. Stottrup, S.L. Veatch, S.L. Keller, Nonequilibrium behavior in supported lipid membranes containing cholesterol, Biophys. J. 86 (2004) 2942–2950.
[75] P. Burgos, C.B. Yuan, M.L. Viriot, L.J. Johnston, Two-color near-field fluorescence microscopy studies of microdomains ("Rafts") in model membranes, Langmuir 19 (2003) 8002–8009.
[76] P.E. Milhiet, M.C. Giocondi, C. Le Grimellec, Cholesterol is not crucial for the existence of microdomains in kidney brush-border membrane models, J. Biol. Chem. 277 (2002) 875–878.
[77] M.C. Giocondi, P.E. Milhiet, P. Dosset, C. Le Grimellec, Use of cyclodextrin for AFM monitoring of model raft formation, Biophys. J. 86 (2004) 861–869.
[78] F. Tokumasu, J. Hwang, J.A. Dvorak, Heterogeneous molecular distribution in supported multicomponent lipid bilayers, Langmuir 20 (2004) 614–618.
[79] F. Tokumasu, A.J. Jin, G.W. Feigenson, J.A. Dvorak, Nanoscopic lipid domain dynamics revealed by atomic force microscopy, Biophys. J. 84 (2003) 2609–2618.
[80] C.D. Blanchette, W.C. Lin, T.V. Ratto, M.L. Longo, Galactosylceramide domain microstructure: impact of cholesterol and nucleation/growth conditions, Biophys. J. 90 (2006) 4466–4478.
[81] C. Yuan, J. Furlong, P. Burgos, L.J. Johnston, The size of lipid rafts: an atomic force microscopy study of ganglioside GM1 domains in sphingomyelin/DOPC/cholesterol membranes, Biophys. J. 82 (2002) 2526–2535.
[82] C.D. Blanchette, W.C. Lin, C.A. Orme, T.V. Ratto, M.L. Longo, Using nucleation rates to determine the interfacial line tension of symmetric and asymmetric lipid bilayer domains, Langmuir 23 (2007) 5875–5877.
[83] C.D. Blanchette, W.C. Lin, C.A. Orme, T.V. Ratto, M.L. Longo, Domain nucleation rates and interfacial line tensions in supported bilayers of ternary mixtures containing galactosylceramide, Biophys. J. 94 (2008) 2691–2697.
[84] C.D. Blanchette, C.A. Orme, T.V. Ratto, M.L. Longo, Quantifying growth of symmetric and asymmetric lipid bilayer domains, Langmuir 24 (2008) 1219–1224.
[85] A.R. Burns, Domain structure in model membrane bilayers investigated by simultaneous atomic force microscopy and fluorescence imaging, Langmuir 19 (2003) 8358–8363.
[86] C.W. Hollars, R.C. Dunn, Submicron structure in L-alpha-dipalmitoylphosphatidylcholine monolayers and bilayers probed with confocal, atomic force, and near–field microscopy, Biophys. J. 75 (1998) 342–353.
[87] T. Kaasgaard, C. Leidy, J.H. Crowe, O.G. Mouritsen, K. Jorgensen, Temperature-controlled structure and kinetics of ripple phases in one- and two-component supported lipid bilayers, Biophys. J. 85 (2003) 350–360.
[88] W.C. Lin, C.D. Blanchette, T.V. Ratto, M.L. Longo, Lipid asymmetry in DLPC/DSPC-supported lipid bilayers: a combined AFM and fluorescence microscopy study, Biophys. J. 90 (2006) 228–237.
[89] C.B. Yuan, L.J. Johnston, Atomic force microscopy studies of ganglioside GM1 domains in phosphatidylcholine and phosphatidylcholine/cholesterol bilayers, Biophys. J. 81 (2001) 1059–1069.
[90] A. Choucair, M. Chakrapani, B. Chakravarthy, J. Katsaras, L.J. Johnston, Preferential accumulation of A beta(1–42) on gel phase domains of lipid bilayers: an AFM and fluorescence study, Biochim. Biophys. Acta 1768 (2007) 146–154.
[91] M.C. Giocondi, V. Vie, E. Lesniewska, P.E. Milhiet, M. Zinke-Allmang, C. Le Grimellec, Phase topology and growth of single domains in lipid bilayers, Langmuir 17 (2001) 1653–1659.
[92] P.I. Kuzmin, S.A. Akimov, Y.A. Chizmadzhev, J. Zimmerberg, F.S. Cohen, Line tension and interaction energies of membrane rafts calculated from lipid splay and tilt, Biophys. J. 88 (2005) 1120–1133.
[93] A.J. García-Sáez, S. Chiantia, P. Schwille, Effect of line tension on the lateral organization of lipid membranes, J. Biol. Chem. 282 (2007) 33537–33544.
[94] S.A. Akimov, P.I. Kuzmin, J. Zimmerberg, F.S. Cohen, Y.A. Chizmadzhev, An elastic theory for line tension at a boundary separating two lipid monolayer regions of different thickness, J. Electroanal. Chem. 564 (2004) 13–18.
[95] H.H. Meyer, Zur Theorie der Alkoholnarkose. Der Einfluss wechselnder Temperature auf Wirkungsstärke und Theilungscoefficient der Narcotica, Arch. Exp. Pathol. Pharmakol. 46 (1901) 338–346.
[96] C.E. Overton, Studien über die Narkose zugleich ein Beitrag zur allgemeinen Pharmakologie, Gustav Fischer, Jena, Switzerland, 1901.
[97] C.E. Overton, Studies of Narcosis, Chapman and Hall, London, 1990.
[98] R.G. Eckenhoff, J.S. Johansson, Molecular interactions between inhaled anesthetics and proteins, Pharmacol. Rev. 49 (1997) 343–367.
[99] J.E. Sirois, Q. Lei, E.M. Talley, C. Lynch III, D.A. Bayliss, The TASK-1 two-pore domain K+ channel is a molecular substrate for neuronal effects of inhalation anesthetics, J. Neurosci. 20 (2000) 6347–6354.
[100] J.W. Tanner, J.S. Johansson, P.A. Liebman, R.G. Eckenhoff, Predictability of weak binding from X-ray crystallography: inhaled anesthetics and myoglobin, Biochemistry 40 (2001) 5075–5080.
[101] R.S. Cantor, The lateral pressure profile in membranes: a physical mechanism of general anesthesia, Biochemistry 36 (1997) 2339–2344.
[102] R.S. Cantor, Lateral pressures in cell membranes: a mechanism for modulation of protein function, J. Phys. Chem., B 101 (1997) 1723–1725.
[103] R.S. Cantor, Breaking the Meyer–Overton rule: predicted effects of varying stiffness and interfacial activity on the intrinsic potency of anesthetics, Biophys. J. 80 (2001) 2284–2297.
[104] E.S. Rowe, Lipid chain length and temperature dependence of ethanol-phosphatidylcholine interactions, Biochemistry 22 (1983) 3299–3305.
[105] E.S. Rowe, Thermodynamic reversibility of phase transitions. Specific effects of alcohols on phosphatidylcholines, Biochim. Biophys. Acta 813 (1985) 321–330.
[106] E.S. Rowe, Induction of lateral phase separations in binary lipid mixtures by alcohol, Biochemistry 26 (1987) 46–51.
[107] S.A. Simon, T.J. McIntosh, Interdigitated hydrocarbon chain packing causes the biphasic transition behavior in lipid/alcohol suspensions, Biochim. Biophys. Acta 773 (1984) 169–172.
[108] J.L. Slater, C.H. Huang, Interdigitated bilayer membranes, Prog. Lipid Res. 27 (1988) 325–359.
[109] H.V. Ly, M.L. Longo, The influence of short-chain alcohols on interfacial tension, mechanical properties, area/molecule, and permeability of fluid lipid bilayers, Biophys. J. 87 (2004) 1013–1033.
[110] A.N. Dickey, R. Faller, Investigating interactions of biomembranes and alcohols: a multiscale approach, J. Polym. Sci. Part B. Polym. Phys. 43 (2005) 1025–1032.
[111] A.N. Dickey, R. Faller, How alcohol chain-length and concentration modulate hydrogen bond formation in a lipid bilayer, Biophys. J. 92 (2007) 2366–2376.
[112] J. Mou, J. Yang, C. Huang, Z. Shao, Alcohol induces interdigitated domains in unilamellar phosphatidylcholine bilayers, Biochemistry 33 (1994) 9981–9985.
[113] R.L. McClain, J.J. Breen, The image-based observation of the LBI-to-LB′ phase transition in solid-supported lipid bilayers, Langmuir 17 (2001) 5121–5124.
[114] Z.V. Leonenko, D.T. Cramb, Revisiting lipid — general anesthetic interactions (I): thinned domain formation in supported planar bilayers induced by halothane and ethanol, Can. J. Chem. 82 (2004) 1128–1138.
[115] A. Carnini, H.A. Phillips, L.G. Shamrakov, D.T. Cramb, Revisiting lipid — general anesthetic interactions (II): halothane location and changes in lipid bilayer microenvironment monitored by fluorescence, Can. J. Chem. 82 (2004) 1139–1149.
[116] L.G. Shamrakov, D.T. Cramb, Induced structural changes of a supported planar bilayer after exposure to halothane — a real-time atomic force microscopy study, Can. J. Chem. 83 (8) (2005) 1190–1194.
[117] Z. Leonenko, E. Finot, D. Cramb, AFM study of interaction forces in supported planar DPPC bilayers in the presence of general anesthetic halothane, Biochim. Biophys. Acta 1758 (2006) 487–492.
[118] H. Alexandre, C. Charpentier, Biochemical aspects of stuck and sluggish fermentation in grape must, J. Ind. Microbiol. Biotech. 20 (1998) 20–27.
[119] E. Canetta, A.K. Adya, G.M. Walker, Atomic force microscopic study of the effects of ethanol on yeast cell surface morphology, FEMS Microbiol. Lett. 255 (2006) 308–315.
[120] K.E. Kirat, Y.F. Dufrêne, L. Lins, R. Brasseur, The SIV tilted peptide induces cylindrical reverse micelles in supported lipid bilayers, Biochemistry (Mosc.) 45 (2006) 9336–9341.
[121] G. Andre, R. Brasseur, Y.F. Dufrêne, Probing the interaction forces between hydrophobic peptides and supported lipid bilayers by AFM, J. Mol. Recognit. 20 (2007) 538–545.
[122] F.A. Carneiro, P.A. Lapido-Loureiro, S.M. Cordo, F. Stauffer, G. Weissmüller, M.L. Bianconi, M.A. Juliano, L. Juliano, P.M. Bisch, A.T.Da. Poian, Probing the interaction between vesicular stomatitis and phosphatidylserine, Eur. Biophys. J. 35 (2006) 145–154.

[123] A.J. García-Sáez, S. Chiantia, J. Salgado, P. Schwille, Pore formation by a bax-derived peptide: effect on the line tension of the membrane probed by AFM, Biophys. J. 93 (2007) 103–112.
[124] H.X. You, L. Yu, X. Qi, Phospholipid membrane restructuring induced by saposin C: a topographic study using atomic force microscopy, FEBS Lett. 503 (2001) 97–102.
[125] H.X. You, X. Qi, L. Yu, Direct AFM observation of saposin C-induced membrane domains in lipid bilayers: from simple to complex lipid mixtures, Chem. Phys. Lipids 132 (2004) 15–22.
[126] J. Murray, L. Cuccia, A. Ianoul, J.J. Cheetham, L.J. Johnston, Imaging the selective binding of synapsin to anionic membrane domains, ChemBioChem 5 (2004) 1489–1494.
[127] M.C. Giocondi, F. Besson, P. Dosset, P. Milhiet, C.L. Grimellec, Remodeling of ordered membrane domains by GPI-anchored intestinal alkaline phosphatase, Langmuir 23 (2007) 9358–9364.
[128] M.C. Giocondi, F. Besson, P. Dosset, P.E. Milhiet, C.L. Grimellec, Temperature-dependent localization of GPI-anchored intestinal alkaline phosphatase in model rafts, J. Mol. Recognit. 20 (2007) 531–537.
[129] S. Chiantia, J. Ries, N. Kahya, P. Schwille, Combined AFM and two-focus SFCS study of raft-exhibiting model membranes, ChemPhysChem 7 (2006) 2409–2418.
[130] D.J. Müller, A. Engel, U. Matthey, T. Meier, P. Dimroth, K. Suda, Observing membrane protein diffusion at subnanometer resolution, J. Mol. Biol. 327 (2003) 925–930.
[131] T. Hughes, B. Strongin, F.P. Gao, V. Vijayvergia, D.D. Busath, AFM visualization of mobile influenza A M2 molecules in planar bilayers, Biophys. J. 87 (2004) 311–322.
[132] D.J. Müller, H. Janovjak, T. Lehto, L. Kuerschner, K. Anderson, Observing structure, function and assembly of single proteins by AFM, Prog. Biophys. Mol. Biol. 79 (2002) 1–43.
[133] A. Engel, D.J. Müller, Observing single biomolecules at work with the atomic force microscope, Nat. Struct. Biol. 7 (2000) 715–718.
[134] S. Scheuring, D. Fotiadis, C. Möller, S.A. Müller, A. Engel, D.J. Müller, Single proteins observed by atomic force microscopy, Single Mol. 2 (2001) 59–67.
[135] M.A. Hussain, A. Agnihotri, C.A. Siedlecki, AFM imaging of ligand binding to platelet integrin $\alpha_{IIb}\beta_3$ receptors reconstituted into planar lipid bilayers, Langmuir 21 (2005) 6979–6986.
[136] P.E. Milhiet, F. Gubellini, A. Berquand, P. Dosset, J.L. Rigaud, C.L. Grimellec, D. Lévy, High-resolution AFM of membrane proteins directly incorporated at high density in planar lipid bilayer, Biophys. J. 91 (2006) 3268–3275.
[137] T. Danker, M. Mazzanti, R. Tonini, A. Rakowska, H. Oberleithner, Using atomic force microscopy to investigate patch-clamped nuclear membrane, Cell Biol. Int. 21 (1997) 747–757.
[138] J.K. Hörber, J. Mosbacher, W. Häberle, J.P. Ruppersberg, B. Sakmann, A look at membrane patches with a scanning force microscope, Biophys. J. 68 (1995) 1687–1693.
[139] J. Mosbacher, M. Langer, J.K. Hörber, F. Sachs, Voltage-dependent membrane displacements measured by atomic force microscopy, J. Gen. Physiol. 111 (1998) 65–74.
[140] E. Pamir, M. George, N. Fertig, M. Benoit, Planar patch-clamp force microscopy on living cells, Ultramicroscopy 108 (2008) 552–557.
[141] P.C. Zhang, A.M. Keleshian, F. Sachs, Voltage-induced membrane movement, Nature 413 (2001) 428–432.
[142] A.J. Bard, F.R.F. Fan, J. Kwak, O. Lev, Scanning electrochemical microscopy. Introduction and principles, Anal. Chem. 61 (1989) 132–138.
[143] A.J. Bard, F.-R.F. Fan, D.T. Pierce, P.R. Unwin, D.O. Wipf, F. Zhou, Chemical imaging of surfaces with the scanning electrochemical microscope, Science 254 (1991) 68–74.
[144] R.C. Engstrom, T. Meaney, R. Tople, R.M. Wightman, Spatiotemporal description of the diffusion layer with a microelectrode probe, Anal. Chem. 59 (1987) 2005–2010.
[145] R.C. Engstrom, M. Weber, D.J. Wunder, R. Burgess, S. Winquist, Measurements within the diffusion layer using a microelectrode probe, Anal. Chem. 58 (1986) 844–848.
[146] C.E. Gardner, J.V. Macpherson, Atomic force microscopy probes go electrochemical, Anal. Chem. 74 (2002) 576A–584A.
[147] J. Abbou, C. Demaille, M. Druet, J. Moiroux, Fabrication of submicrometer-sized gold electrodes of controlled geometry for scanning electrochemical-atomic force microscopy, Anal. Chem. 74 (2002) 6355–6363.
[148] D.P. Burt, N.R. Wilson, J.M.R. Weaver, P.S. Dobson, J.V. Macpherson, Nanowire probes for high resolution combined scanning electrochemical microscopy — atomic force microscopy, Nano Lett. 5 (2005) 639–643.
[149] C. Kranz, G. Friedbacher, B. Mizaikoff, A. Lugstein, J. Smoliner, E. Bertagnolli, Integrating an ultramicroelectrode in an AFM cantilever: combined technology for enhanced information, Anal. Chem. 73 (2001) 2491–2500.
[150] A. Lugstein, E. Bertagnolli, C. Kranz, A. Kueng, B. Mizaikoff, Integrating micro- and nanoelectrodes into atomic force microscopy cantilevers using focused ion beam techniques, Appl. Phys. Lett. 81 (2002) 349–351.
[151] J.V. Macpherson, P.R. Unwin, Combined scanning electrochemical-atomic force microscopy, Anal. Chem. 72 (2000) 276–285.
[152] C. Kranz, A. Kueng, A. Lugstein, E. Bertagnolli, B. Mizaikoff, Mapping of enzyme activity by detection of enzymatic products during AFM imaging with integrated SECM-AFM probes, Ultramicroscopy 100 (2004) 127–134.
[153] A. Kueng, C. Kranz, A. Lugstein, E. Bertagnolli, B. Mizaikoff, AFM-tip-integrated amperometric microbiosensors: high-resolution imaging of membrane transport, Angew. Chem., Int. Ed. 44 (2005) 3419–3422.
[154] A.P. Quist, A. Chand, S. Ramachandran, C. Daraio, S. Jin, R. Lal, Atomic force microscopy imaging and electrical recording of lipid bilayers supported over microfabricated silicon chip nanopores: lab-on-a-chip system for lipid membranes and ion channels, Langmuir 23 (2007) 1375–1380.